Desalination and Water Treatment
www.deswater.com
doi: 10.5004/dwt.2023.29616

298 (2023) 61–74
June

Excellent adsorption ability of Hg(II) by poly(o-phenylenediamine) modified mesoporous materials

Xuyin Lin[a], Jinwen Jiang[b], Jun Wang[a], Jiaofen Lin[a], Aikebaier Reheman[a,c,*]

[a]*Xiamen Ocean Vocational College, Xiamen 361100, China, emails: akbarphd@126.com (A. Reheman), xmhy000@163.com (X. Lin), wangjun@xmoc.edu.cn (J. Wang), 183588136@qq.com (J. Lin)*
[b]*College of Science, Northeastern University, Shenyang 110819, China, email: 1164513332@qq.com (J. Jiang)*
[c]*Fujian Key Laboratory of Toxicant and Drug Toxicology, Medical College, Ningde Normal University, Ningde, Fujian 352100, China*

Received 5 February 2023; Accepted 26 May 2023

ABSTRACT

In this study, we used mesoporous silica materials as inorganic carrier and poly(o-phenylenediamine) with more active amino and imino groups as organic ligand to obtain functionalized adsorbent. The composite adsorbent poly(o-phenylenediamine) modified mesoporous composites (MPP) were prepared by loading poly(o-phenylenediamine) onto the surface of the aminated mesoporous material through *in-situ* polymerization. It was found that the maximum saturation adsorption capacity of MPP reached 225 mg/g when the solution pH, temperature, initial Hg(II) concentration, and adsorption time were 4, 298.15 K, 100 mg/L, and 240 min, respectively. When common interfering ions Zn(II), Ni(II), Cu(II), Ca(II), Mg(II) and Al(III) were present, the adsorption of Hg(II) by MPP still showed good selectivity. The adsorption of Hg(II) by MPP followed quasi-secondary kinetics and the Langmuir adsorption isotherm model, indicating that the adsorption process was chemisorption. In addition, MPP removed up to 81.35% of Hg(II) from industrial wastewater. After five cycles for adsorbent regeneration experiments, the adsorption capacity of MPP could reach 191.67 mg/g, indicating that the adsorbent has good regeneration performance and potential application value for removal of Hg(II).

Keywords: Mesoporous silica materials; Poly(o-phenylenediamine); Composite adsorbent; Adsorption; Hg(II)

1. Introduction

Water is the basic material of all life, the protection and management of water resources is the basic guarantee of people's healthy life [1]. According to the different pollutants, water pollution can be broadly divided into chemical pollution, physical pollution, biological pollution, of which the impact of chemical pollution has become more and more intense [2,3]. Due to the rapid development of modern industry, the pollution of heavy metals in water bodies has become increasingly serious, posing a serious threat to the living environment of human beings, especially mercury, a heavy metal with strong toxicity and difficult degradability [4–6]. With the Minamata Convention in full swing in 2017, mercury ion pollution in wastewater has become an important issue related to human life and health. Mercury ions in aqueous solutions can enter the food chain even at very low concentrations and accumulate in aquatic organisms and eventually in the human body through the consumption of fish and other marine substances [7–9]. Mercury poisoning can damage the liver, brain function, nervous system, and reproductive system and cause a variety of biological and genetic diseases [10–12]. However, most of the current mercury ion adsorbents have many disadvantages, such as low adsorption capacity, high cost and difficult regeneration [13–15]. How to treat and efficiently purify heavy metal mercury in water is still the focus of research.

* Corresponding author.

The U.S. Environmental Protection Agency (EPA) advises against consuming water with Hg(II) concentrations more than 0.002 mg/L (2 ppb) [16]. Therefore, for human safety, mercury contamination in water must be treated before releasing heavy metal ion effluent into the environment [17]. To address this problem, researchers have developed a variety of methods to combat mercury contamination: chemical precipitation, microbial methods, organic chelation, ion exchange, and membrane separation [18–22]. However, these technologies always have disadvantages such as poor removal capacity, low metal removal rate, secondary pollution, etc. [23]. Therefore, there is a need to explore a cost-effective technology to treat mercury contamination. Adsorption is recognized as a cost-effective water treatment method because of its relatively simple operation, high removal capacity and low cost [24].

Mesoporous silica materials have high specific surface area, adjustable pore size and shape, and rich morphological structure, so they can be used as excellent carriers. It is widely used in adsorption, catalysis, sensors and other directions due to its good functional properties and occupies a very important position in many scientific and technological fields [25]. Bui et al. [26] successfully synthesized mesoporous molecular sieves using coal ash (CBA) as a substrate. To find the ideal conditions for silica extraction from CBA powder, several calcination temperatures and different sodium hydroxide and CBA ratios were examined in alkali synthesis [26]. The results showed that mesoporous silica materials (MCM-41) could be used as an effective and reasonably priced adsorbent for the removal of heavy metal ions from wastewater because it could be synthesized under ideal conditions and had a specific surface area of 932 m^2/g, a pore volume of 0.93 cm^3/g, and a pore size of 3.14 nm [26]. According to reported research [27], MCM-41 with amino functionality was utilized as an adsorbent to remove the antibiotic ciprofloxacin, and MCM-41 with diamine functionality had a higher capacity for chemical monolayer adsorption because it contained more amino-activated groups on its surface. This study shows that mesoporous silica materials have promising applications in the field of adsorption and reveals their adsorption and desorption behavior [27].

In recent years, researchers have proposed a variety of methods for the preparation of poly(o-phenylenediamine) micro- and nanomaterials [28]. The main synthetic methods include chemical oxidation, hydrothermal, electroformation, solid-phase synthesis and microwave-assisted methods [29]. Poly(o-phenylenediamine) micro and nanostructures in spherical, ribbon and other morphologies were synthesized by these methods [30]. Since poly(o-phenylenediamine) contains free amino groups and adjacent imine groups in its molecular chain, it can form a stable complex structure, which has a strong chelating effect on heavy metal ions in solution, and adsorbs these heavy metal ions in water to the polymer well [31]. Shi et al. [32] synthesized poly(o-phenylenediamine) pellets by chemical oxidation method using ammonium persulfate as oxidant. It also showed good adsorption capacity for both Ag(I) and Pb(II), with a saturation capacity of 195.5 mg/g for Pb(II) and 540 mg/g for Ag(I), and was able to reduce silver ions to monolithic nano-silver at the same time [28]. Aromatic diamine polymers show promising applications because of their simple synthesis process and their strong heavy metal ion binding ability.

In this study, the MPP composite adsorbent was firstly obtained by loading poly(o-phenylenediamine) onto the surface of the aminated mesoporous material by *in-situ* polymerization using MCM-41 as the inorganic carrier and poly(o-phenylenediamine) as the organic ligand. Since poly-phenylenediamine contains a large amount of active amino and imino groups, it enhances the chelating effect of the adsorbent on heavy metal ions and the adsorption capacity and mechanical stability of the adsorbent. The morphology, structure and chemical properties of the adsorbent were characterized by Fourier-transform infrared spectroscopy (FTIR), X-ray powder diffraction (XRD), thermogravimetric analysis (TGA), scanning electron microscopy (SEM) etc. On the adsorption of Hg(II) in water, the impacts of several variables including pH, adsorption time, starting Hg(II) concentration, adsorption temperature, and co-existing ions were examined, and the optimal adsorption conditions were explored. Secondly, the adsorbent was experimentally investigated for adsorption cycle regeneration. Finally, the experimental data were fitted kinetically and thermodynamically to investigate the adsorption mechanism of the adsorbent. As a result, a new and effective adsorbent for the removal of Hg(II) ions was created. It has a large supply of raw materials, is inexpensive, and has a quick preparation process cycle, so it may be used to remove Hg(II) ions from actual industrial effluent.

2. Experimental set-up

2.1. Materials and instruments

Details on the instruments and materials are provided in the supporting documents (Text S1).

2.2. Preparation of MPP

2.2.1. Preparation of MCM-41

Firstly, 5 g of diatomaceous earth powder (200 mesh) was dispersed in 20 mL of a solution with a concentration of 40% H_2SO_4, sonicated, and mechanically stirred for 8 h. The mixed solution was filtered to obtain the solid. Then, the filtered solid was washed with water several times and dried in a vacuum oven at 100°C for 24 h. The dried solid was calcined in a muffle furnace at a temperature of 450°C for 4 h. Next, 2.7 g of pretreated diatomaceous earth with 1.02 g NaOH and 25 mL of H_2O was heated and refluxed in a 100 mL bottom flask for 4 h. After heating, the afore-mentioned combination was added to a cetyltrimethylammonium bromide (CTAB) solution (3.06 g CTAB, 51 mL water), where it was agitated for 1 h. Then, the precursor was moved to a stainless-steel autoclave and heated to 100°C for 24 h after H_2SO_4 (2 mol/L) was used to bring the solution's pH to 10. After the reaction, filtering, repeated washings with ethanol solution and deionized water, and 12 h of drying at 60°C were used to achieve the white precipitate. Finally, to remove the CTAB template from the pores, the white precipitate was calcined at 550°C for 6 h to obtain MCM-41.

2.2.2. Preparation of MCM-41-NH_2

Prior to adding 2.5 mL of ammonia dropwise, 1 g of MCM-41 was added to a flask holding 100 mL of pyridine. The mixture was then sonicated for 30 min. After sonication, 1 mL of 3-aminopropyltriethoxysilane (KH550) was slowly added dropwise to the mixed solution under N_2 protection. Then, the mixture was rapidly agitated for 24 h at room temperature in a nitrogen environment. After that, the suspension was filtered. The resulting material was repeatedly cleaned with ethanol and deionized water before being dried for 12 h in a vacuum oven at 45°C. Finally, MCM-41-NH_2 was successfully obtained, as shown in Fig. 1.

2.2.3. Preparation of MPP

90 mL of distilled water was mixed with 0.5 g of MCM-41-NH_2, and the mixture was then sonicated for 30 min. When the system was dispersed more uniformly, a certain amount of o-phenylenediamine solid was added to it and stirred for 30 min until all the o-phenylenediamine solid was dissolved in the system. 10 mL of distilled water were used to dissolve a certain amount of sodium persulfate to create a solution that would serve as the reaction's catalyst. Ammonium persulfate solution was slowly dropped into the above solution under argon gas as a protective gas, and the whole system was placed in an ice bath for 8 h. Following the reaction, the solution was filtered, the solid that was produced was repeatedly washed with deionized water and ethanol, and the solid was then freeze-dried for 12 h in a vacuum freezer. Finally, the poly(o-phenylenediamine) modified mesoporous composites (MPP) were obtained. The preparation process is shown in Fig. 1.

2.3. Adsorption experiment

MPP adsorbent was used to perform the adsorption studies of Hg(II) ions, including some adsorption parameters such as pH, adsorption time, initial Hg(II) ion concentration, adsorption temperature and the effect of interfering ions. Firstly, Different quantities of Hg(II) solutions (100–500 mg/L) were created by dilution from a Hg(II) ion stock solution with a standard concentration of 1,000 mg/L. The initial solution pH was adjusted to 1~7 with 0.8 mol/L of HNO_3 and NaOH, and Hg(II) ion solutions of different pH (100 mg/L, 50 mL) were mixed with 0.02 g of MPP adsorbent at 298 K. The effect on the adsorption was investigated by controlling different pH, adsorption time, temperature, and interfering ions. 5 mL of Hg(II) ion solution was taken and 0.02 g of adsorbent was added to it after a certain time of adsorption. 4 mL of the adsorbed solution was taken in a centrifuge tube and separated by centrifugation. 1 mL of the supernatant after centrifugation was taken in a 25 mL volumetric flask. Using dithizone spectrophotometry, the amount of Hg(II) ions in the supernatant was measured. The adsorption amount and removal rate of Hg(II) ions by the adsorbent were calculated according to Eqs. (1) and (2) [33].

$$Q_t = \frac{(C_0 - C_t)\cdot V}{m} \tag{1}$$

$$R = \frac{(C_0 - C_t)}{C_0} \times 100\% \tag{2}$$

where Q_t (mg/L) is the adsorption amount at equilibrium, m is the mass of the adsorbent (g), V is the volume of the solution (L), and R is the removal rate of Hg(II) ions from the solution (%). C_0 and C_t are the concentration of Hg(II) ions in the solution (mg/L) before and after adsorption, respectively.

3. Results and discussion

3.1. Characterization

3.1.1. FTIR analysis

Fig. 2A shows the FTIR spectra of MCM-41, MCM-41-NH_2 and MPP, respectively. From the FTIR spectrum of MCM-41, it can be seen that the peak at 3,659 cm^{-1} characteristic peak is attributed to the stretching vibration of surface silanol (Si–OH), while the stretching vibrations at 1,080 and 800 cm^{-1} are caused by the asymmetric stretching of Si–O–Si and symmetric stretching [34]. From the FTIR spectrum of MCM-41-NH_2, it can be concluded that the stretching vibration peak of Si–OH disappears after the mesoporous MCM-41 is modified with amino groups. The asymmetric and symmetric stretching vibration absorption peaks of –CH_2– are represented by the absorption peaks at 2,920 and 2,860 cm^{-1}, respectively. The peaks at

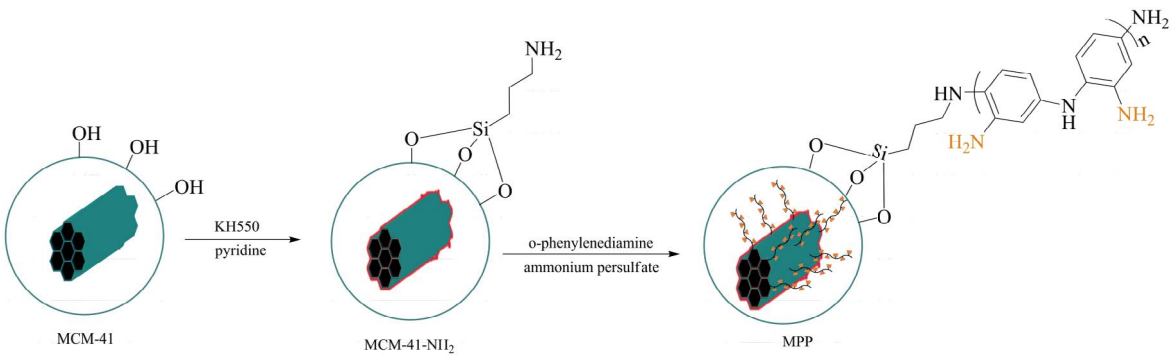

Fig. 1. Preparation depiction of MPP.

1,568 and 1,465 cm^{-1} are attributed to the stretching vibration of the $–NH_2$ group. These observations confirm that the organic part of KH550 has been successfully transposed to MCM-41 [35,36]. The peaks at 3,420 and 3,195 cm^{-1} in the FTIR spectrum of MPP correspond to the N–H stretching vibrations of the –NH– and $–NH_2$ groups, and the peak at 1,620 cm^{-1} is a bending stretching vibration peak in the N–H plane. The absorption peak at 1,305 cm^{-1}, on the other hand, is a stretching vibration absorption peak of benzene ring –C–N [37], indicating that poly(o-phenylenediamine) has been successfully loaded onto the MCM-41-NH_2 structure. Besides, the results of FTIR characterization of the adsorbed materials before and after adsorption are shown in Fig. 2C. The comparison shows that there is a more obvious –NH– stretching vibration peak at 3,420 cm^{-1} before adsorption, but the –NH– characteristic peak is significantly weakened after adsorption. It indicates that the –NH-functional group in MPP binds to Hg(II) ions during the adsorption process.

3.1.2. XRD analysis

The XRD patterns of MCM-41, MCM-41-NH_2, and MPP are depicted in Fig. 2B. Among them, MCM-41 showed diffraction peaks at 2.47°, 4.32° and 5.13°, respectively, and corresponded to the (100), (110) and (200) crystallographic planes of the cubic structure of MCM-41, which is consistent with the characteristic diffraction peak of MCM-41 reported in the literature [38,39]. Moreover, although the intensity of the peaks of MCM-41-NH_2 and MPP gradually decreased due to the amination of MCM-41 and the grafting of the polymer, the main characteristic peaks were still present, which indicated that the final synthesized MPP still had a well-ordered structure.

3.1.3. TGA analysis

Fig. 2D shows the TGA curves of MCM-41, MCM-41-NH_2 and MPP. As can be seen that the mass loss of the three TGA profiles at the first stage (below 150°C) could be correlated with the weight loss of the bound water on the material surface. Additionally, each sample's mass loss from 150°C to 600°C may be ascribed to the mass loss of its organic functional groups. The TGA curve of MCM-41 showed that the weight loss of the material was 3.78% between 40°C and 150°C and virtually stayed constant between 150°C and 600°C, demonstrating that the material had high thermal stability. The TGA curve of MCM-41-NH_2 showed a weight loss of 9.21% in the temperature range of 150°C–600°C, which can be attributed to the thermogravimetric loss of organic matter loaded on the surface of MCM-41, indicating that KH550 has successfully functionalized MCM-41. By comparing TGA curves of MCM-41-NH_2 and MPP, it was found that there was a 14.73% weight loss difference

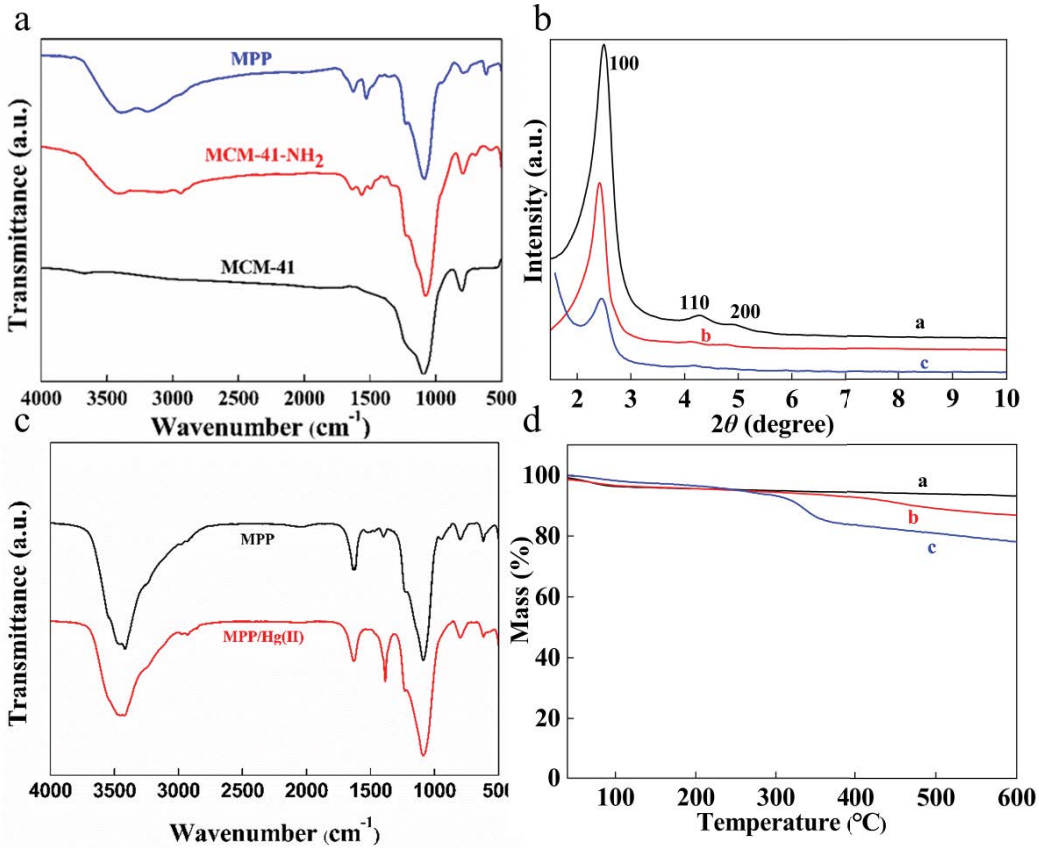

Fig. 2. (A) FTIR spectra of MCM-41, MCM-41-NH_2 and MPP, (B) X-ray powder diffraction patterns of MCM-41 (a), MCM-41-NH_2 (b) and MPP (c), (C) FTIR spectra of MPP and MPP/Hg(II), and (D) thermogravimetric analysis curves of MCM-41 (a), MCM-41-NH_2 (b) and MPP (c).

between the two compounds, indicating that poly(o-phenylenediamine) had been immobilized on the mesoporous silica surface by an *in-situ* polymerization process, and the MPP composite adsorbent had been successfully prepared.

3.1.4. SEM and transmission electron microscopy analysis

Fig. 3 shows SEM and transmission electron microscopy images of MCM-41, MCM-41-NH_2 and MPP, respectively. The clearer morphology of silica particles in MCM-41 can be seen in Fig. 3a, and MCM-41-NH_2 in Fig. 3b exhibits interconnected nanoparticle surfaces due to silylation. Compared with MCM-41 in Fig. 3a and MCM-41-NH_2 in Fig. 3b, the surface of MPP in Fig. 3c became rougher and more dense, indicating that the poly(o-phenylenediamine) polymer had been loaded onto the surface of MCM-41-NH_2. Fig. 3d shows that the mesoporous pore channels of MCM-41 were more clearly distributed. It can be illustrated in Fig. 3e that the amination of MCM-41 did not affect the pore structure of the mesopores. Fig. 3f shows clearly that the mesoporous surface was loaded with a layer of polymer, demonstrating that a large amount of poly(o-phenylenediamine) particles were loaded onto the surface of MCM-41-NH_2.

3.1.5. Brunauer–Emmett–Teller analysis

To determine the specific surface area, pore volume, and pore size distribution of the adsorbents, N_2 desorption studies were carried out on the MCM-41, MCM-41-NH_2, and MPP adsorbents, respectively. The results are displayed in Fig. 4, and Table S1 lists the related physical property data. As can be obtained in Fig. 4, the adsorption isotherms of all

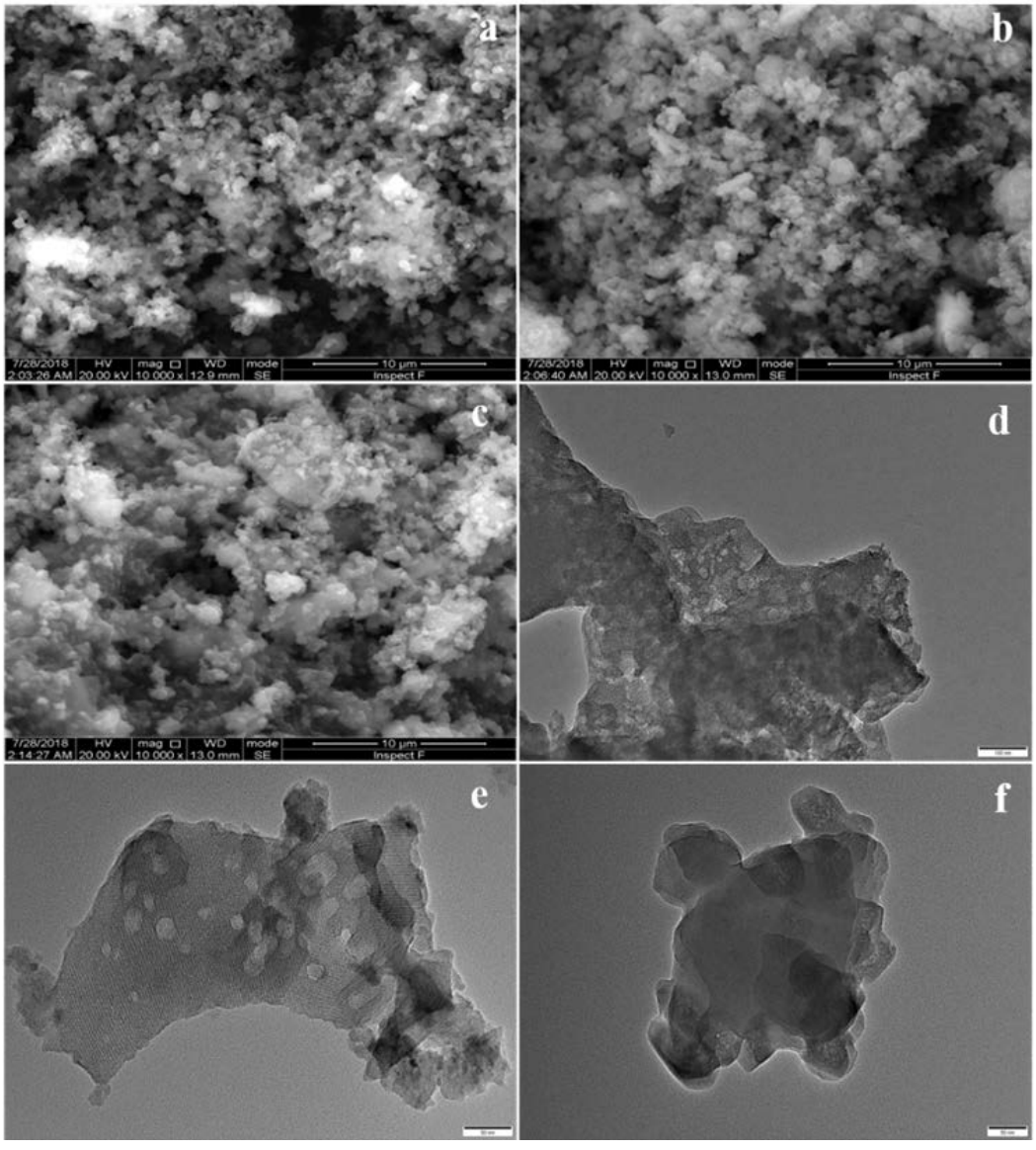

Fig. 3. Scanning electron microscopy images of MCM-41 (a), MCM-41-NH_2 (b) and MPP (c), transmission electron microscopy images of MCM-41 (d), MCM-41-NH_2 (e) and MPP (f).

samples conform to the type IV curve, which is consistent with literature reports [40,41] and is typical of the MCM-41 nitrogen desorption isotherm. It can be seen that with the increase of relative pressure, comparing MCM-41, MCM-41-NH_2, MPP does not undergo a sharp jump, mainly due to the modification of poly(o-phenylenediamine) which reduces the orderliness of the mesoporous structure. By comparison to MCM-41 (793.51 m^2/g), the surface areas of MCM-41-NH_2 and MPP were decreased to 257.12 and 77.27 m^2/g, respectively. In contrast to MCM-41 (0.59 cm^3/g), the pore volumes of MCM-41-NH_2 and MPP were 0.59 and 0.123 cm^3/g, respectively. Contrarily, compared to the MCM-41 (3.26 nm), the pore size of MCM-41-NH_2 increased to 4.59 nm due to particle interconnections and the creation of new macropores, while that of MPP decreased to 1.93 nm, indicating the successful polymerization of poly(o-phenylenediamine) on MCM-41-NH_2.

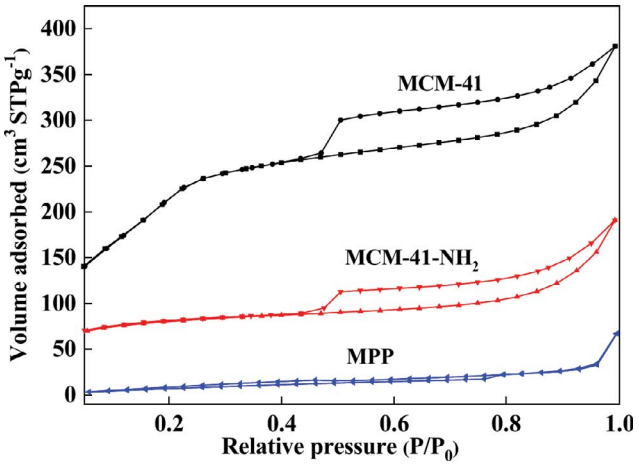

Fig. 4. N_2 adsorption–desorption curves for MCM-41, MCM-41-NH_2 and MPP.

3.2. Effect of pH on adsorption behavior

One of the crucial variables in the process of adsorption is the pH variation since it has an important impact on the level of metal ionization and the metal binding sites on the adsorbent surface [42]. According to Fig. 5, the adsorption capacity of the adsorbent greatly increased as the pH of the solution grew from 1 to 4, but it gradually declined as the pH of the solution increased from 4 to 7. The reason for this was mainly due to the larger H^+ concentration in the more acidic solution, while the zeta potential value on the MPP surface decreased continuously with increasing pH during the whole process. The above phenomenon can be explained as follows: The primary cause is the system's low pH and high concentration of H^+ in the solution, which causes the amino and hydroxyl functional groups on the adsorbent's surface to get protonate. Due to protonation, the surface of MPP carries a high positive zeta potential, resulting in a relatively strong electrostatic repulsion between it and Hg(II) ions, making it difficult for Hg(II) to bind to the adsorption site on the surface of the adsorbent and greatly reducing the ability to bind to Hg(II). The amount of H^+ in

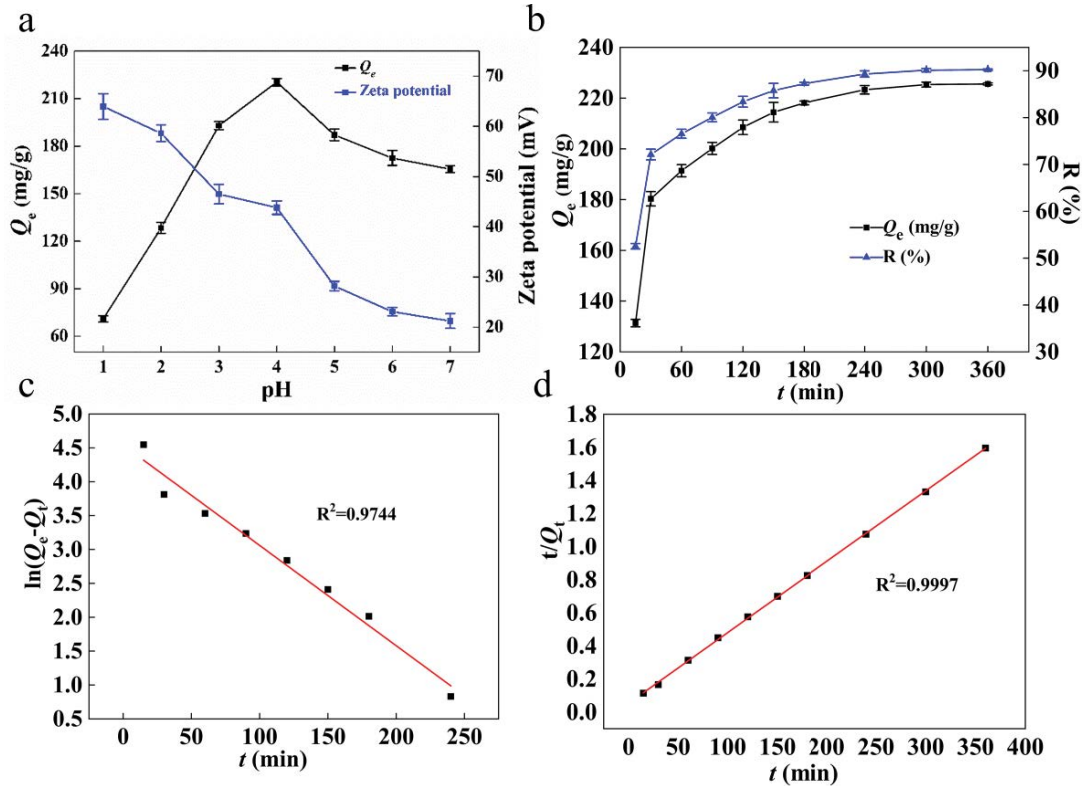

Fig. 5. (a) Effect of pH on Hg(II) adsorption and zeta potential of MPP, (b) effect of contact time on the adsorption of Hg(II) ions, (c) quasi-first-order kinetic curve and (d) quasi-second-order kinetic curve.

the solution steadily reduced as pH rose, and a large number of amino functional groups were exposed, making the adsorbent surface stronger in binding to Hg(II). The decrease in the protonation of the functional groups of MPP is consistent with the sharp decrease in the zeta potential. On the other hand, when the pH was greater than 4, the OH^- concentration of the solution increased, causing the gradual conversion of Hg(II) in solution to the forms of $Hg(OH)^+$ and $Hg(OH)_2$ [43,44]. The $Hg(OH)^+$ and $Hg(OH)_2$ produced on the adsorbent surface block the mesopores and binding sites because they typically have a lower positive charge and a lower affinity for functional groups, which causes the adsorption capacity to progressively decline. In summary, the optimal pH for Hg(II) adsorption by MPP adsorbent is 4. And for the study of Hg(II) ion adsorption, 100 mg/L of Hg(II) ion solution, adsorption time of 240 min, pH of 4 and room temperature were used as the optimal adsorption conditions.

3.3. Effect of contact time on adsorption behavior and adsorption kinetics

3.3.1. Effect of contact time on adsorption behavior

Fig. 5b shows that the adsorption quantity rose quickly over time in the early stage from 0 to 60 min, but that from 60 to 240 min, the adsorption rate steadily declined until the adsorption saturation condition was attained. The reason for this phenomenon was the presence of a large number of amino and imino active functional groups on the surface of the adsorbent at the beginning of the adsorption phase, which could rapidly bind to Hg(II) and therefore the adsorption amount increased rapidly. However, a large amount of Hg(II) was combined with the functional group, and the surface of the functional group would have a large amount of positive charge, which made the Hg(II) adsorbed on the surface of the adsorbent and the free Hg(II) in the solution appear to repel each other with the same charge, so the adsorption rate decreased slowly and reaches the saturation adsorption amount of 225 mg/g (RSD = 0.791) at 240 min.

Additionally, 90 mL of distilled water was mixed with 0.5 g of MCM-41-NH_2 before being sonicated for 30 min. After the system was more evenly distributed, o-phenylenediamine solids were added at concentrations of 1.2, 2.4, 3.6, and 4.8 mmol, and the MPP composite adsorbent was synthesized under the condition of ammonium persulfate as initiator. The prepared adsorbent was added to 100 mL of Hg(II) standard solution at a concentration of 50 mg/L, respectively, and adsorbed for 240 min with magnetic stirring on a magnetic stirring rotary table. Dithizone spectrophotometry was used to measure the concentration of Hg(II) in the adsorbed solution after the adsorption was complete. The results are displayed in Fig. S1. It can be seen that the best adsorption effect of MPP adsorbent was achieved when the o-phenylenediamine was fed at 2.4 mmol.

3.3.2. Adsorption kinetics

A quasi-first-order kinetic model and a quasi-second-order kinetic model are required to investigate the adsorption mechanism and fit the maximum adsorption capacity of the adsorbent to research the adsorption process and mechanism of this adsorbent. Eqs. (3) and (4) describe the pseudo-first-order and pseudo-second-order models, respectively.

$$\ln\left(Q_e - Q_t\right) = \ln Q_e - k_1 t \tag{3}$$

$$\frac{t}{Q_t} = \frac{1}{k_2 Q_e^2} + \frac{1}{Q_e} \tag{4}$$

where the Hg(II) adsorption capacity at time t and equilibrium time are indicated by the units Q_t and Q_e (mg/g), respectively. The rate constants k_1 for pseudo-first-order models and k_2 for pseudo-second-order models are both used in mathematical models.

The kinetic data for the adsorption of Hg(II) by the adsorbent were fitted with a quasi-primary kinetic model and a quasi-secondary kinetic model, and the results of the fitted data are shown in Fig. 5c and d. As can be seen from Table S2, the fitted correlation coefficient of the quasi primary kinetic model is low, and the deviation of the fitted maximum adsorption amount from the actual adsorption amount is large, indicating that the adsorption of Hg(II) on the adsorbent does not conform to the quasi primary kinetics. According to the quasi-secondary kinetic model, the fitted correlation coefficient was high (R^2 = 0.9997) and the fitted maximum adsorption amount of 233.64 mg/g was in general agreement with the actual adsorption amount of 225.33 mg/g. This suggests that the adsorption of Hg(II) by MPP composite adsorbent may be well described by the quasi-secondary kinetic equation.

3.4. Effect of Hg(II) concentration and adsorption isotherm

3.4.1. Effect of Hg(II) concentration

If the initial Hg(II) concentration was increased from 100 to 200 mg/L, it is evident from Fig. 6a that the quantity of Hg(II) that the adsorbent could bind to rise as well. The saturation adsorption capacity did not change significantly with the continued increase of the initial Hg(II) concentration. The primary cause of this occurrence was the presence of more active functional groups on the surface of the adsorbent in low Hg(II) concentrations, which allowed for the efficient chelation of significant amounts of Hg(II). Although there was a strong driving force between Hg(II) in solution and the adsorbent when the Hg(II) concentration was 200 mg/L, the quantity of active sites on the adsorbent's surface were restricted, and the amount of Hg(II) ions adsorbed finally stabilized. Therefore, the adsorption capacity did not increase greatly when the Hg(II) concentration was larger, and the adsorbent had reached the saturation adsorption state at this time, and the corresponding saturation adsorption capacity is 331.64 mg/g. Table S3 compares the maximum adsorption capacity of several types of adsorbents for Hg(II) and shows that MPP has superior adsorption quality.

3.4.2. Adsorption isotherm

To further investigate the relationship between the adsorbent and the adsorbent mass during adsorption, the

adsorption behavior of the adsorbent was explored by means of the Hg(II) adsorption isotherm, and the Langmuir and Freundlich adsorption isotherm equations were commonly used to describe the adsorption process [45,46]. Among them, the Langmuir adsorption isotherm is used to describe the homogeneous adsorption of single molecular layers; the Freundlich adsorption isotherm assumes non-homogeneous surface adsorption with uneven heat distribution of surface adsorption. The Langmuir and Freundlich model are expressed as Eqs. (5) and (6).

$$\frac{C_e}{Q_e} = \frac{1}{Q_m K_L} + \frac{C_e}{Q_m} \tag{5}$$

$$\ln Q_e = \ln K_F + \frac{1}{n} \ln C_e \tag{6}$$

where C_e (mg/L) is the equilibrium adsorption concentration; Q_e (mg/g) is the equilibrium adsorption volume; Q_m (mg/g) is the adsorption capacity of the saturated monomolecular layer, the larger this parameter predicts the larger adsorption capacity of the adsorbent. K_F and K_L are the Freundlich and Langmuir adsorption constants, respectively; n is a constant indicating the adsorption index.

From the data in Fig. 6b & c and Table S4, it can be seen that the determined coefficient R^2 of the Langmuir model for Hg(II) adsorption of this adsorbent was higher than that of the Freundlich model, and the theoretical maximum adsorption amount fitted by the Langmuir model was basically consistent with the actual measured values, indicating that the adsorption isotherm for Hg(II) of this adsorbent was more consistent with the Langmuir adsorption isotherm model. The Langmuir model assumes that the

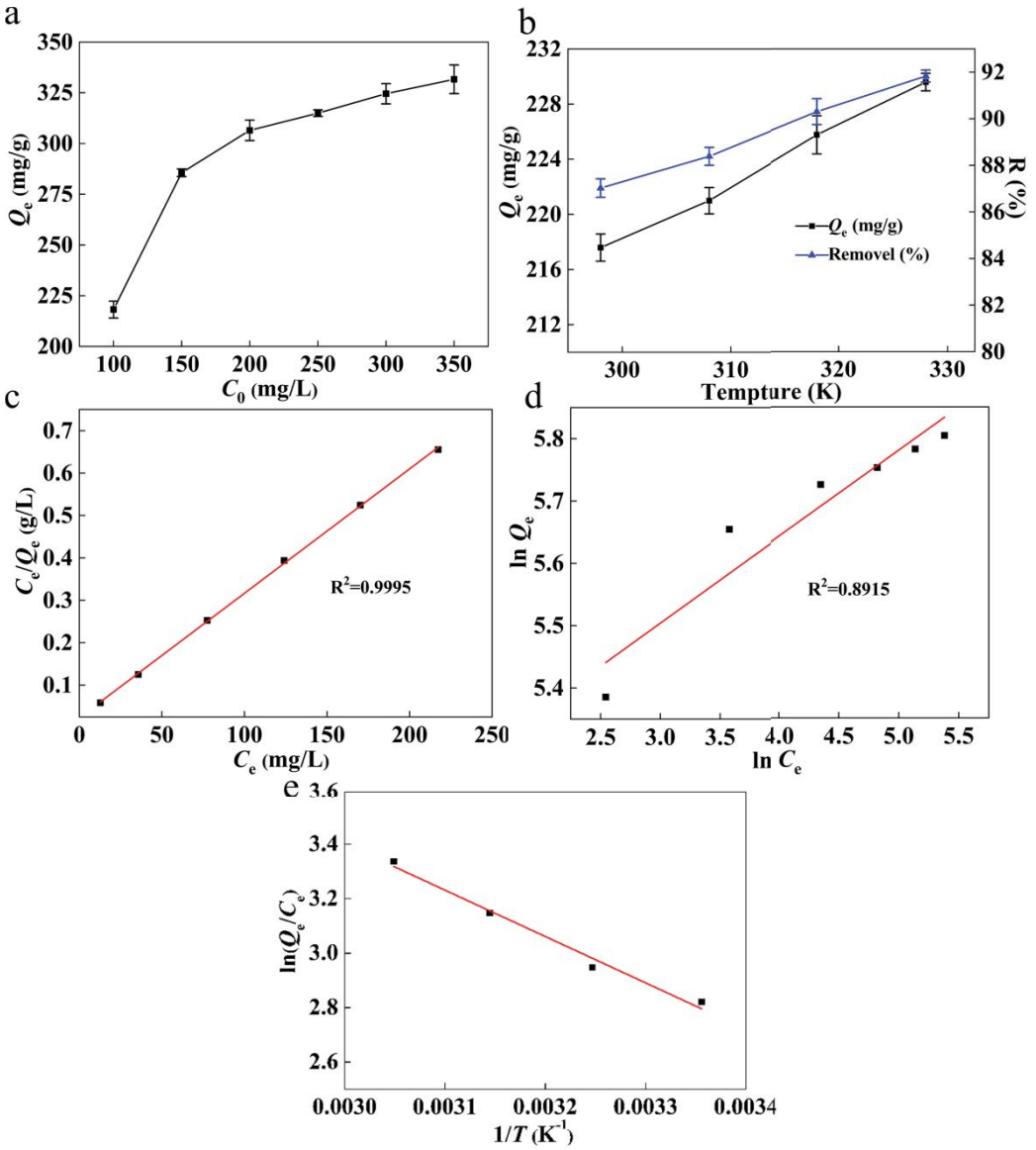

Fig. 6. (a) Effect of initial Hg(II) ion concentration on the sorption, (b) effect of temperature on Hg(II) adsorption, (c) Langmuir isotherm plots for the adsorption of Hg(II) ion onto MPP, (d) Freundlich isotherm plots for the adsorption of Hg(II) ion onto MPP and (e) relationship between $\ln(Q_e/C_e)$ and $1/T$.

adsorbent relies on the active sites on its surface for monolayer adsorption. Therefore, the monolayer adsorption of Hg(II) by MPP was dependent on active centers on the adsorbent surface, such as hydroxyl and amino groups.

3.5. Effect of temperature and thermodynamic study

To investigate the effect of temperature on the adsorption effect of MPP composite adsorbent, and its adsorption effect at different temperatures, the experimental data were linearly fitted using the Van't Hoff equation, the expression of which is as follows.

$$\ln\left(\frac{Q_e}{C_e}\right) = \frac{-\Delta H^\circ}{RT} + \frac{\Delta S^\circ}{R} \tag{7}$$

$$\Delta G^\circ = -RT \cdot \ln\left(\frac{Q_e}{C_e}\right) \tag{8}$$

where ΔG° is the Gibb's free energy, ΔH° is the enthalpy change and ΔS° entropy change. The value of ΔG° is calculated by using the data to determine whether the reaction is spontaneous or not, and the value of ΔH° enthalpy change is calculated to determine the heat change of the adsorption process.

The enthalpy change ΔH° = 12.45 kJ/mol and entropy change ΔS° = 70.77 J/mol·K, and the corresponding Gibb's free energy ΔG° at different temperatures can be calculated from the results of the data fitted to Fig. 6b and e, as shown in Table S5. From the data in the above table, it can be seen that the Gibb's free energy ΔG° is negative at different temperatures, and the enthalpy change $\Delta H^\circ > 0$ is derived from the thermodynamically fitted data, indicating that the adsorption of Hg(II) by the MPP composite adsorbent is a spontaneous heat absorption process.

3.6. Effect of co-existed ions and application in industrial wastewater

In the process of adsorbing Hg(II) from wastewater, it is necessary to explore whether the adsorbent is selective for the adsorption of Hg(II) when other metal ions are present in the system due to the presence of a large number of other impurity metal ions in the wastewater. In the presence of various cations, such as Zn(II), Ni(II), Cu(II), Ca(II), Mg(II), and Al(III), weighed MPP (0.02 g) was added to 50 mL of 100 mg/L Hg(II) solution at an initial concentration of 0.01 M. The adsorption of MPP on Hg(II) was measured, and the corresponding results are shown in Fig. 7a. The interfering ions in the solution had no effect on MPP's ability to adsorb Hg(II) ions, demonstrating high selectivity of MPP. To investigate the removal ability of MPP adsorbent on Hg(II) ions in industrial wastewater, a high concentration of industrial wastewater with a concentration of 480 mg/L was taken and diluted to 100 mg/L, 50 mL of it was taken and the pH was adjusted to 4. Then 0.02 g of MPP adsorbent was added and adsorbed under magnetic stirring for 240 min, and finally the removal rate of MPP adsorbent on mercury ions in industrial wastewater was measured to be 81.35%. It shows that MPP adsorbent has good adsorption potential for industrial wastewater.

3.7. Regeneration study

As a functional adsorbent, in addition to its efficient adsorption performance, its reusability is also an important indicator to assess the performance of the adsorbent. A mixture of nitric acid (0.2 mol/L) and thiourea (0.1 mol/L) was used as the eluent of the adsorbent, and the eluted adsorbent was freeze-dried, after which the results of repeated multiple adsorption tests were performed as shown in Fig. 7b. The results showed that the adsorption capacity of the recovered MPP composite adsorbent for Hg(II) reached 191.39 mg/g after five cycles. The loss of adsorbent material during the adsorbent recovery process throughout the repeated studies may be the cause of the decline in adsorption capacity, however the adsorption capacity fundamentally remained stable. Therefore, the MPP composite adsorbent exhibited good regeneration performance as well as potential applications in the adsorption process.

3.8. Possible adsorption mechanism of Hg(II) ions

To further investigate the adsorption mechanism of Hg(II) ions by MPP, the changes in the chemical

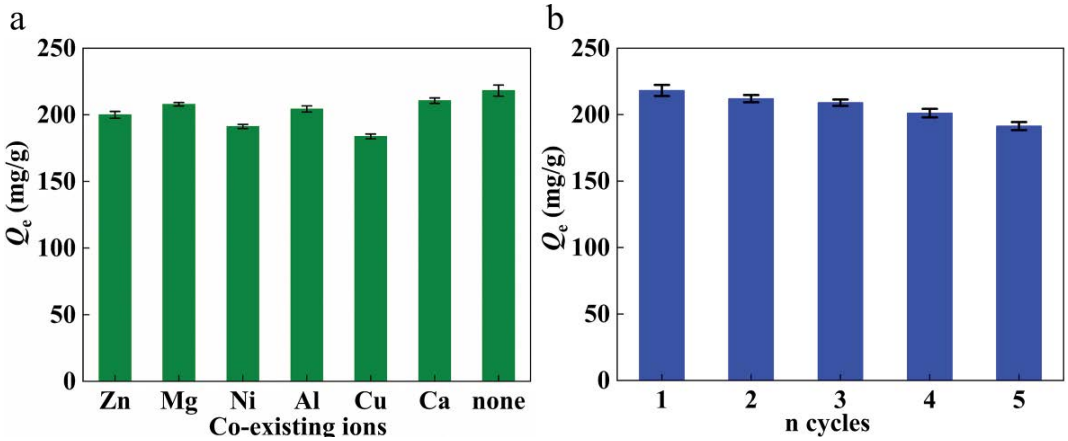

Fig. 7. (a) Effect of co-existing ions in solution on Hg(II) adsorption and (b) regeneration behavior of absorbent.

environment of the relevant elements before and after the adsorption of Hg(II) in water by MPP adsorbent were analyzed by X-ray photoelectron spectroscopy (XPS), and the test results are shown in Fig. 8a. By comparing the full-spectrum scanned spectra of MPP adsorbent before and after adsorption, new characteristic peaks of Hg4f, Hg4d5, and Hg4d3 could be observed in the XPS spectra of MPP/Hg(II) after adsorption, and these characteristic peaks indicated that MPP adsorbent had successfully adsorbed Hg(II). Further high-resolution XPS scans were performed for elemental mercury and the results are shown in Fig. 8b, with the presence of characteristic peaks at 100.93 and 104.67 eV in the high-resolution spectrum of Hg4f, corresponding to the Hg4f7/2 and Hg4f5/2 characteristic peaks, respectively [47]. In addition, the MPP adsorbent contains a large number of organic functional groups including –NH–, $–NH_2$. The high-resolution XPS spectra of C1s and N1 were further examined to investigate the impact of the included C and N elemental functional groups on the adsorption of Hg(II). The results are displayed in Fig. 8c and d. Fig. 8c(i) shows three characteristic peaks for C–N, C–C and C=C with corresponding binding energies of 286.08, 285.03 and 284.28 eV, respectively. Comparison with Fig. 8c(ii) revealed a smaller change in the characteristic peak displacement and intensity of the corresponding C1s of MPP/Hg(II) after the adsorption of Hg(II), indicating that C–N, C–C and C=C functional groups play a role in the adsorption of Hg(II) ions. The characteristic peaks of –NH– and $–NH_2$ appear in the high-resolution spectra of N1s in Fig. 8d(i) with binding energies of 401.63 and 399.23 eV, respectively. However, after the adsorption of Hg(II), the binding energies of the corresponding peaks of –NH– and $–NH_2$ in the high-resolution spectra of N1s change to 401.53 and 399.03 eV. The intensity of the peaks after the adsorption of Hg(II) and the position of the peaks changed, indicating a strong interaction between N in the –NH– or $–NH_2$ functional groups and Hg(II).

Based on the kinetic model and isothermal adsorption model, the adsorption of mercury ions by MPP may involve ligand chelation of functional groups, complexation reaction, ion exchange and other adsorption effects, and its adsorption mechanism is shown in Fig. 9. First, MPP can rapidly remove Hg(II) ions from solution through the metal chelation reaction of amino ($–NH_2$) and imino (–NH–) in the

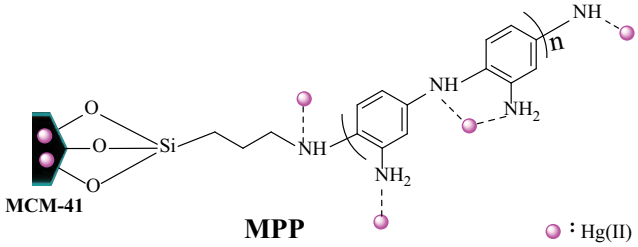

Fig. 9. Adsorption mechanism of Hg(II) ions removed by MPP.

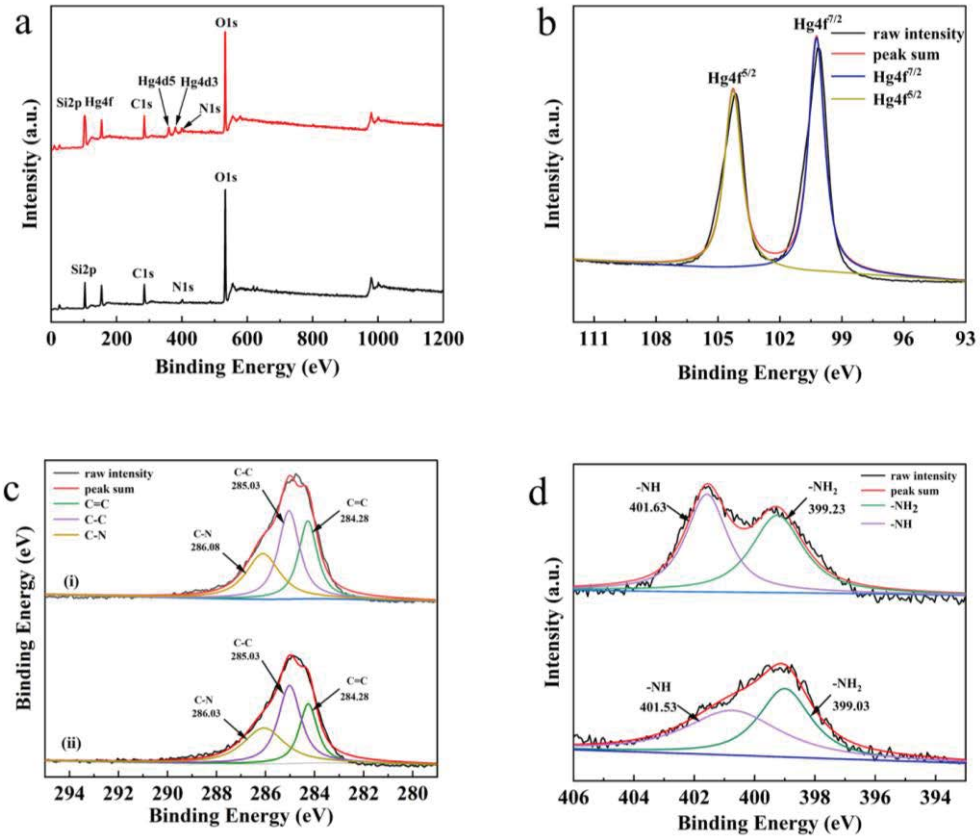

Fig. 8. (a) Full survey XPS spectra, high-resolution Hg 4f (b), C1s (c), N1s (d) of MPP before (i) and after Hg(II) adsorption (ii).

molecular backbone of poly(o-phenylenediamine). Secondly, MPP can also play an important role in the adsorption of Hg(II) through complexation reaction of NH_2 and –NH– with Hg(II) also, while NH_2 can also undergo ion exchange reaction with Hg(II) ions to achieve the purpose of adsorption of Hg(II). Finally, Hg(II) ions may also move from the MPP surface to the pores through intracrystalline diffusion when the active site is saturated, and they may then be electrostatically attracted to the silica hydroxyl groups on the mesoporous surface and trapped there.

4. Conclusions

In this study, MCM-41 was used as an inorganic carrier, and the MCM-41-NH_2 inorganic carrier was obtained by amination modification. Subsequently, the poly(o-phenylenediamine)-modified mesoporous composite was obtained by *in-situ* polymerization using o-phenylenediamine as monomer and ammonium persulfate as initiator. It was found that the adsorbent not only had a high specific surface area, but also contained a large number of reactive groups on its surface, which can quickly and highly selectively remove mercury ions from the solution. The best adsorption effect of MPP was achieved at pH = 4, adsorption temperature of 298.15 K, initial Hg(II) concentration of 100 mg/g, and adsorption time of 240 min with a saturation adsorption capacity of 225 mg/g and a corresponding removal rate of 90%. Interference ion experiment shows that the adsorbent has good selective adsorption of Hg(II), and MPP still has high removal rate for Hg(II) adsorption in industrial wastewater. The adsorption capacity of MPP could still reach 191.39 mg/g after 5 cycles of regeneration experiments, and the adsorbent showed good regeneration performance. The thermodynamic study found that ΔG was negative and ΔH was positive at each temperature, indicating that the adsorption of Hg(II) by the MPP composite adsorbent was a spontaneous heat absorption process. In summary, the adsorbent has a simple preparation process, high adsorption capacity, and good selectivity and reusability, which can be used to effectively remove mercury ions from wastewater.

Declaration of competing interest

The authors declare that they have no known competing financial interests or personal relationships that could have appeared to influence the work reported in this paper.

Data availability

Data will be made available on request.

Acknowledgement

This work was supported by Fujian Marine Economic Development Special project (FJHJF-L-2022-21) and Scientific Research Fund project of Ningde Normal University (2020Z02).

References

[1] K. Makanda, S. Nzama, T. Kanyerere, Assessing the role of water resources protection practice for sustainable water resources management: a review, Water, 14 (2022) 3153, doi: 10.3390/w14193153.
[2] A.A. Alqadami, S.M. Wabaidur, B.H. Jeon, M.A. Khan, Co-hydrothermal valorization of food waste: process optimization, characterization, and water decolorization application, Biomass Convers. Biorefin., (2023), doi: 10.1007/s13399-022-03711-7.
[3] I. Ali, O.M.L. Alharbi, Z.A. ALOthman, A.M. Al-Mohaimeed, A. Alwarthan, Modeling of fenuron pesticide adsorption on CNTs for mechanistic insight and removal in water, Environ. Res., 170 (2019) 389–397.
[4] A. Chaturvedi, S. Bhattacharjee, A.K. Singh, V. Kumar, A new approach for indexing groundwater heavy metal pollution, Ecol. Indic., 87 (2018) 323–331.
[5] M. Asim, K.N. Rao, Assessment of heavy metal pollution in Yamuna River, Delhi-NCR, using heavy metal pollution index and GIS, Environ. Monit. Assess., 193 (2021) 103, doi: 10.1007/s10661-021-08886-6.
[6] A. Liu, Y. Ma, J.M.A. Gunawardena, P. Egodawatta, G.A. Ayoko, A. Goonetilleke, Heavy metals transport pathways: the importance of atmospheric pollution contributing to stormwater pollution, Ecotoxicol. Environ. Saf., 164 (2018) 696–703.
[7] K.G. Pavithra, P. SundarRajan, P.S. Kumar, G. Rangasamy, Mercury sources, contaminations, mercury cycle, detection and treatment techniques: a review, Chemosphere, 312 (2023) 137314, doi: 10.1016/j.chemosphere.2022.137314.
[8] Y. Bolaños-Álvarez, C.M. Alonso-Hernández, R. Morabito, M. Díaz-Asencio, V. Pinto, M. Gómez-Batista, Mercury contamination of riverine sediments in the vicinity of a mercury cell chlor-alkali plant in Sagua River, Cuba, Chemosphere, 152 (2016) 376–382.
[9] M.M. Al-Sulaiti, L. Soubra, M.A. Al-Ghouti, The causes and effects of mercury and methylmercury contamination in the marine environment: a review, Curr. Pollut. Rep., 8 (2022) 249–272.
[10] R. Siblerud, J. Mutter, E. Moore, J. Naumann, H. Walach, A hypothesis and evidence that mercury may be an etiological factor in Alzheimer's disease, Int. J. Environ. Res. Public Health, 16 (2019) 5152, doi: 10.3390/ijerph16245152.
[11] M. Tuzen, A. Sarı, M.R.A. Mogaddam, S. Kaya, K.P. Katin, N. Altunay, Synthesis of carbon modified with polymer of diethylenetriamine and trimesoyl chloride for the dual removal of Hg(II) and methyl mercury ($[CH_3Hg]^+$) from wastewater: Theoretical and experimental analyses, Mater. Chem. Phys., 277 (2022) 125501, doi: 10.1016/j.matchemphys.2021.125501.
[12] Naeemullah, M. Tuzen, A. Sarı, I. Turkekul, Influential bioremoval of mercury using *Lactarius acerrimus* macrofungus as novel low-cost biosorbent from aqueous solution: isotherm modeling, kinetic and thermodynamic investigations, Mater. Chem. Phys., 24 (2020) 123168, doi: 10.1016/j.matchemphys.2020.123168.
[13] T. Velempini, K. Pillay, Sulphur functionalized materials for Hg(II) adsorption: a review, J. Environ. Chem. Eng., 7 (2019) 103350, doi: 10.1016/j.jece.2019.103350.
[14] T.A. Saleh, A. Sarı, M. Tuzen, Optimization of parameters with experimental design for the adsorption of mercury using polyethylenimine modified-activated carbon, J. Environ. Chem. Eng., 5 (2017) 1079–1088.
[15] T.A. Saleh, M. Tuzen, A. Sarı, Polyamide magnetic palygorskite for the simultaneous removal of Hg(II) and methyl mercury; with factorial design analysis, J. Environ. Manage., 211 (2018) 323–333.
[16] G.K. Kinuthia, V. Ngure, D. Beti, R. Lugalia, A. Wangila, L. Kamau, Levels of heavy metals in wastewater and soil samples from open drainage channels in Nairobi, Kenya: community health implication, Sci. Rep., 10 (2020) 8434, doi: 10.1038/s41598-020-65359-5.
[17] J.C. Wasserman, L. de Oliveira Silva, G.C. de Pontes, E. de Paiva Lima, Mercury contamination in the sludge of drinking water treatment plants dumping into a reservoir in Rio de Janeiro, Brazil, Environ. Sci. Pollut. Res., 25 (2018) 28713–28724.
[18] M.A. Khan, S.M. Wabaidur, M.R. Siddiqui, A.A. Alqadami, A.H. Khan, Silico-manganese fumes waste encapsulated

cryogenic alginate beads for aqueous environment de-colorization, J. Cleaner Prod., 244 (2020) 118867, doi: 10.1016/j.jclepro.2019.118867.
[19] N.A. AlFaris, S.M. Wabaidur, Z.A. Alothman, J.Z. Altamimi, T.S. Aldayel, Fast and efficient immunoaffinity column cleanup and liquid chromatography–tandem mass spectrometry method for the quantitative analysis of aflatoxins in baby food and feeds, J. Sep. Sci., 43 (2020) 2079–2087.
[20] A. Azhar, Y. Yamauchi, A.E. Allah, Z.A. Alothman, A.Y. Badjah, M. Naushad, M. Habila, S. Wabaidur, J. Wang, M.B. Zakaria, Nanoporous iron oxide/carbon composites through *in-situ* deposition of Prussian blue nanoparticles on graphene oxide nanosheets and subsequent thermal treatment for supercapacitor applications, Nanomaterials, 9 (2019) 776, doi: 10.3390/nano9050776.
[21] Z.A. ALOthman, S.M. Wabaidur, Application of carbon nanotubes in extraction and chromatographic analysis: a review, Arabian J. Chem., 12 (2019) 633–651.
[22] H. Ahmad, R. Ahmad Khan, B. Heun Koo, A. Alsalme, Cellulose nanofibers@ZrO_2 membrane for the separation of Hg(II) from aqueous media, J. Phys. Chem. Solids, 168 (2022) 110812, doi: 10.1016/j.jpcs.2022.110812.
[23] H. Sadegh, G.A.M. Ali, A.S.H. Makhlouf, K.F. Chong, N.S. Alharbi, S. Agarwal, V.K. Gupta, MWCNTs-Fe_3O_4 nanocomposite for Hg(II) high adsorption efficiency, J. Mol. Liq., 258 (2018) 345–353.
[24] M. Arshadi, H. Eskandarloo, M. Karimi Abdolmaleki, A. Abbaspourrad, A biocompatible nanodendrimer for efficient adsorption and reduction of Hg(II), ACS Sustainable Chem. Eng., 6 (2018) 13332–13348.
[25] A. Marjani, R. Soltani, M. Pishnamazi, M. Rezakazemi, S. Shirazian, Functionalized pollen-like mesoporous silica, Microporous Mesoporous Mater., 310 (2021) 110531, doi: 10.1016/j.micromeso.2020.110531.
[26] D.-H. Vu, H.-B. Bui, X.-N. Bui, D. An-Nguyen, Q.-T. Le, N.-H. Do, H. Nguyen, A novel approach in adsorption of heavy metal ions from aqueous solution using synthesized MCM-41 from coal bottom ash, Int. J. Environ. Anal. Chem., 100 (2020) 1226–1244.
[27] D. Lu, S. Xu, W. Qiu, Y. Sun, X. Liu, J. Yang, J. Ma, Adsorption and desorption behaviors of antibiotic ciprofloxacin on functionalized spherical MCM-41 for water treatment, J. Cleaner Prod., 264 (2020) 121644, doi: 10.1016/j.jclepro.2020.121644.
[28] M. Baibarac, M. Daescu, E. Matei, D. Nastac, O. Cramariuc, Optical properties of composites based on poly(o-phenylenediamine), poly(vinylene fluoride) and double-wall carbon nanotubes, Int. J. Mol. Sci., 22 (2021) 8260, doi: 10.3390/ijms22158260.
[29] S. Jadoun, U. Riaz, J. Yáñez, N. Pal Singh Chauhan, Synthesis, characterization and potential applications of poly(o-phenylenediamine) based copolymers and nanocomposites: a comprehensive review, Eur. Polym. J., 156 (2021) 110600, doi: 10.1016/j.eurpolymj.2021.110600.
[30] N. Kannapiran, A. Muthusamy, P. Chitra, S. Anand, R. Jayaprakash, Poly(o-phenylenediamine)/$NiCoFe_2O_4$ nanocomposites: synthesis, characterization, magnetic and dielectric properties, J. Magn. Magn. Mater., 423 (2017) 208–216.
[31] Y. Meng, L. Xiao, A. Muslim, M. Hojiahmat, Improving the adsorption of poly(o-phenylenediamine) to heavy metal ions in aqueous solution through its composite with carbon dots, J. Polym. Res., 28 (2021) 404, doi: 10.1007/s10965-021-02739-z.
[32] M. Shi, Y. Peng, J. Zhou, B. Liu, Y. Huang, J. Kong, Multianalyte immunoassay based on insulating-controllable PoPD film at arrayed electrodes integrated on a silicon chip, Biosens. Bioelectron., 22 (2007) 2841–2847.
[33] Z.A. Alothman, A.H. Bahkali, M.A. Khiyami, S.M. Alfadulc, S.M. Alfadul, S.M. Wabaidur, M. AlamLow, B.Z. Alfarhan, Low cost biosorbents from fungi for heavy metals removal from wastewater, Sep. Sci. Technol., 55 (2020) 1766–1775.
[34] G. Mohammadnezhad, S. Abad, R. Soltani, M. Dinari, Study on thermal, mechanical and adsorption properties of amine-functionalized MCM-41/PMMA and MCM-41/PS nanocomposites prepared by ultrasonic irradiation, Ultrason. Sonochem., 39 (2017) 765–773.
[35] J. Zhou, Y. Li, H.-b. Sun, Z. Tang, L. Qi, L. Liu, Y. Ai, S. Li, Z. Shao, Q. Liang, Porous silica-encapsulated and magnetically recoverable Rh NPs: a highly efficient, stable and green catalyst for catalytic transfer hydrogenation with "slow-release" of stoichiometric hydrazine in water, Green Chem., 19 (2017) 3400–3407.
[36] C. Laslau, Z.D. Zujovic, L. Zhang, G.A. Bowmaker, J. Travas-Sejdic, Morphological evolution of self-assembled polyaniline nanostuctures obtained by pH-stat chemical oxidation, Chem. Mater., 21 (2009) 954–962.
[37] W. Liu, J. Kumar, S. Tripathy, L.A. Samuelson, Enzymatic synthesis of conducting polyaniline in micelle solutions, Langmuir, 18 (2002) 9696–9704.
[38] D. Kumar, K. Schumacher, C. du Fresne von Hohenesche, M. Grün, K.K. Unger, MCM-41, MCM-48 and related mesoporous adsorbents: their synthesis and characterisation, Colloids Surf., A, 187–188 (2001) 109–116.
[39] D.M. Marzouqa, M.B. Zughul, M.O. Taha, H.A. Hodali, Effect of particle morphology and pore size on the release kinetics of ephedrine from mesoporous MCM-41 materials, J. Porous Mater., 19 (2012) 825–833.
[40] J. Rouquerol, D. Avnir, C.W. Fairbridge, D.H. Everett, J.M. Haynes, N. Pernicone, J.D.F. Ramsay, K.S.W. Sing, K.K. Unger, Recommendations for the characterization of porous solids (Technical Report), Pure Appl. Chem., 66 (1994) 1739–1758.
[41] A. Jafarzadeh, S. Sohrabnezhad, M.A. Zanjanchi, M. Arvand, Synthesis and characterization of thiol-functionalized MCM-41 nanofibers and its application as photocatalyst, Microporous Mesoporous Mater., 236 (2016) 109–119.
[42] Y. Liu, Q. Li, X. Cao, Y. Wang, X. Jiang, M. Li, M. Hua, Z. Zhang, Removal of uranium(VI) from aqueous solutions by CMK-3 and its polymer composite, Appl. Surf. Sci., 285 (2013) 258–266.
[43] S. Pan, Y. Zhang, H. Shen, M. Hu, An intensive study on the magnetic effect of mercapto-functionalized nano-magnetic Fe_3O_4 polymers and their adsorption mechanism for the removal of Hg(II) from aqueous solution, Chem. Eng. J., 210 (2012) 564–574.
[44] A. Walcarius, C. Delacôte, Mercury(II) binding to thiol-functionalized mesoporous silicas: critical effect of pH and sorbent properties on capacity and selectivity, Anal. Chim. Acta, 547 (2005) 3–13.
[45] I. Langmuir, The adsorption of gases on plane surfaces of glass, mica and platinum, J. Am. Chem. Soc., 40 (1918) 1361–1403.
[46] N. Ballav, R. Das, S. Giri, A.M. Muliwa, K. Pillay, A. Maity, l-cysteine doped polypyrrole (PPy@L-Cyst): a super adsorbent for the rapid removal of Hg^{+2} and efficient catalytic activity of the spent adsorbent for reuse, Chem. Eng. J., 345 (2018) 621–630.
[47] S. Zeng, L. Li, L. Xie, D. Zhao, N. Wang, S. Chen, Conducting polymers crosslinked with sulfur as cathode materials for high-rate, ultralong-life lithium–sulfur batteries, ChemSusChem, 10 (2017) 3378–3386.

Supporting information

S1. Details of materials and instruments

Diatomaceous earth, hydrochloric acid, cetyltrimethylammonium bromide, pyridine 3-aminopropyltriethoxysilane (KH550), o-phenylenediamine, sodium hydroxide, dithizone, mercury nitrate, nitric acid, anhydrous ethanol Tralatone was purchased from Tianjin Damao Chemical Reagent Factory (Tianjin, China). Ammonium persulfate purchased from Aladdin Industries (Shanghai, China) Fourier-transform infrared spectroscopy spectra were recorded on a PerkinElmer spectrometer (Waltham, Massachusetts, USA) using KBr particles in the range of 4,000–500 cm^{-1}. X-ray powder diffraction spectra of the samples were obtained with Cu-Kα radiation (λ = 1.54 Å) in the range of 1°–10° (2θ) at 40 kV and 40 mA. The morphology of the samples was observed by scanning electron microscopy (JEOL 6500F, Tokyo, Japan) and transmission electron microscopy (JEM-2000EX). X-ray photoelectron spectroscopy and Brunauer–Emmett–Teller was used to analyze the surface composition of the samples using ESCALAB 250.

Table S1
Surface area, pore diameter and pore volume of MCM-41, MCM-41-NH_2 and MPP

Sample	Surface area (m^2/g)	Pore size (nm)	Pore volume (cm^3/g)
MCM-41	793.51	3.26	0.59
MCM-41-NH_2	257.12	4.59	0.30
MPP	77.27	1.93	0.12

Table S2
Parameters of adsorption kinetic and intraparticle diffusion model

Models	Parameters	Value
Quasi-first-order equation	$Q_{e,(cal)}$ (mg/g)	93.64
	k_1 (min^{-1})	–0.0148
	R^2	0.9744
Quasi-second-order equation	$Q_{e,(cal)}$ (mg/g)	233.64
	k_2 (g/mg·min)	0.000343
	R^2	0.9997

Table S3
Comparison of the maximum adsorption capacities of different kinds of adsorbents on Hg(II) removal

Adsorbents	Q_m (mg/g)	Adsorbent dosage (g/L)	Initial concentration of Hg^{2+} (mg/L)	References
TC-CS	164.80	0.50	5–150	[S1]
MMSP	243.83	0.40	50–300	[S2]
CNTs-SH@Fe_3O_4	172.40	0.50	10–470	[S3]
MPP	331.64	0.40	100–350	This work

Table S4
Langmuir and Freundlich isotherm parameters

Models	Parameters	Value
Langmuir	$Q_{m,cal}$ (mg/g)	341.29
	K_L (L/mg)	0.1256
	R^2	0.9995
Freundlich	K_F	162.0816
	n	7.23
	R^2	0.8915

Table S5
Thermodynamic parameters at different temperatures

T (K)	298	308	318	328
$\Delta G°$ (kJ/mol)	–8.65	–9.36	–10.07	–10.77

Notes: $\Delta H°$ = 12.45 kJ/mol; $\Delta S°$ = 70.77 J/(mol·K).

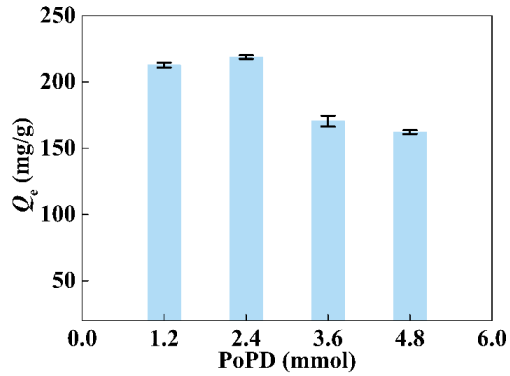

Fig. S1. Effect of the o-phenylenediamine dosage in MPP on the adsorption.

References

[S1] L. Fan, A. Zhou, L. Zhong, Z. Zhang, Y. Liu, Selective and effective adsorption of Hg(II) from aqueous solution over wide pH range by thiol functionalized magnetic carbon nanotubes, Chemosphere, 226 (2019) 405–412.
[S2] J. Sun, Z. Chen, M. Ge, L. Xu, M. Zhai, Selective adsorption of Hg(II) by γ-radiation synthesized silica-graft-vinyl imidazole adsorbent, J. Hazard. Mater., 15 (2013) 94–101.
[S3] W. Liang, M. Li, Z. Zhang, Y. Jiang, M.K. Awasthi, S. Jiang, Decontamination of Hg(II) from aqueous solution using polyamine-*co*-thiourea inarched chitosan gel derivatives, Int. J. Biol. Macromol., 113 (2018) 106–115.